Muon Spin Rotation in Anisotropic Superconductors in an External Magnetic Field

A thesis submitted in partial fulfillment of the requirement
for the degree of Bachelor of Science in
Physics from the College of William and Mary in Virginia,

by

Raymond N. Dickes III

Advisor: Dr. William J. Kossler

Williamsburg, Virginia
May 2001

Abstract

The high T_c, Type II superconductor YBCO is studied in an external magnetic field oriented parallel, perpendicular, and at a 45° angle to the c axis of the unit cell crystal over a range of temperatures. Variations in temperature change the penetration depth of the superconductor. This in turn alters the magnetic field distribution internal to the sample. Muon Spin Rotation (μSR) is capable of determining the probability distribution of these fields and thus may be used to investigate the internal fields. μSR measurements which were carried out at the TRIUMF μSR Facility are analyzed. Four separate fitting functions were used: a gaussian function, to provide a general overview; a London Theory isotropic function for b$\|$c; an anisotropic fitting function more appropriate to high fields; and an anisotropic function that is more appropriate for the low fields used. A comparison is made between these fits. An agreement between the behavior of the penetration depths for the parallel and perpendicular cases is observed which points to the possibility of "Flux Line Pairs."

Acknowledgments

Dr. William J. Kossler, The College of William and Mary

Dr. Chris D. Carone, The College of William and Mary

Contents

1 Introduction

1.1 Motivation

The scientific community has harnessed the power of superconducting materials ever since their discovery at the turn of the century. Allowing for more efficient circuitry and advanced electronics, these materials revolutionized electronic technology. However, the limitations on their superconductivity led physicists to seek alternatives. The discovery of high T_c superconductors was a huge breakthrough in the field of superconductivity. These materials are superconductive at much higher temperatures when compared to previously observed superconductors. This allows for easier experimentation and exploitation of their properties. However, scientists have yet to unravel all of the mysteries behind them. One aspect of these superconductors that could shed new light on their qualities is the structure of their internal magnetic fields. Direct mearsurements on the structure of these fields is possible with muon spin rotation, but current data on the topic is limited. Further knowledge of their behaviors would be greatly beneficial to the understanding of these materials and could promote even further use and benefit.

1.2 Overview

It is thought that the supercurrents that generate the internal magnetic fields are primarily restricted to the molecular planes perpendicular to the c axis in the unit cell crystal. Figure 1 shows the unti cell crystal for the superconductor $YBa_2Cu_3O_{7-\delta}$, abbreviated YBCO. For the past several years the TRIUMF μSR Facility has gathered data on the subject using the method of muon penetration and decay and the subsequent scattering of positrons in a sample of the superconducting material YBCO. The analysis of the data collected from their experiments with μSR scattering in anisotropic superconductors has led to the discovery of some of the more interesting

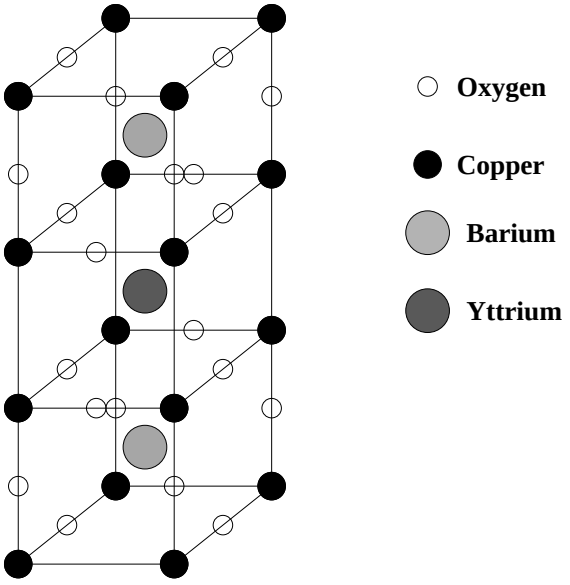

Figure 1: The unit cell crystal for the superconductor YBCO. The CuO_2 planes between the Barium and Yttrium atoms are the location of the supercurrents. The c axis runs perpendicular to these planes. The $Cu - O - Cu$ chains that comprise the axes of these planes represent the a and b axes of the material.

behaviors of the high T_c superconductor YBCO.

Using the phenomenological London Assumption of topological current theory, the asymmetric plots of the positron detector pairs (up/down and left/right) are mapped using an analytical program of Dr. Kossler's own design. Certain situations involving the applied magnetic field's orientation reveal the most information about the material. These situations include influencing the internal fields with: a small magnetic field parallel to the c axis of the material, a small magnetic field perpendicular to the c axis, and a small magnetic field at a 45° angle to the c axis. However, for this paper the last scenario is not included in the comparison because of a lack of variety to the data and need for a better means of fitting. It will be discussed but not in as great of detail as the other two. The experimental setup, the physical data accumulated from the YBCO sample, the fitting program, and the analytical method are covered

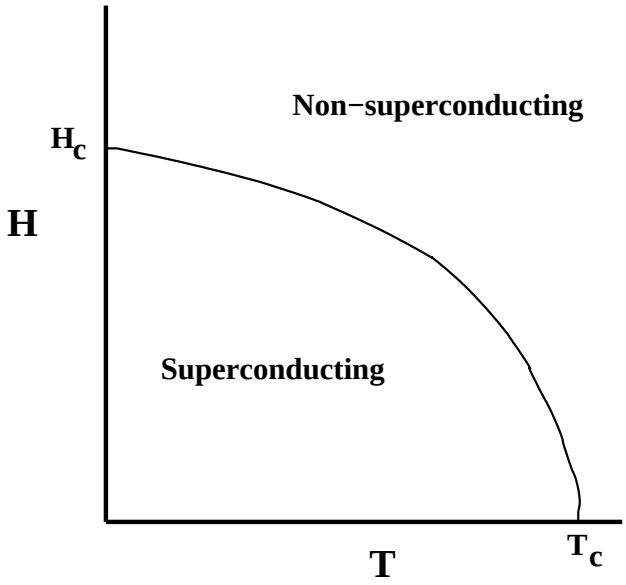

Figure 2: A general representation of a Type I superconductor with relative critical field H_c and critical temperature T_c.

in more detail in sections 3 and 4.

2 Superconductivity

2.1 Type I and Type II Superconductors

Superconductors are composed of two types of materials. The first type, termed Type I, are limited to two physical states. The first state is a superconductive state in which all magnetic fields present in the material are expelled to the surface creating a perfect diamagnet. Under certain conditions with respect to temperature and the magnitude of magnetic fields, such as reaching a critical temperature T_c or a critical field H_c, the material enters a second state in which the material loses its superconductivity completely. Figure 2 shows the relationship between Temperature and Magnetic field for a Type I superconductor.

Type II superconductors are able to be in one of three different states. The first

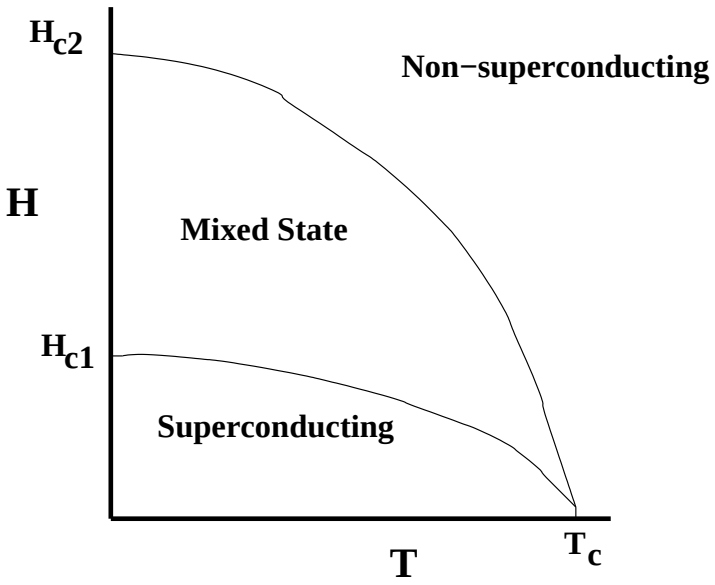

Figure 3: A general represenation of a Type II superconductor with relative critical fields H_{c1} and H_{c2} and critical temperature T_c.

state for a Type II material is exactly the same as the first state for a Type I material but generally ends at a lower H_c than most Type I materials. After the first critical field H_{c1} is reached the material enters into its second state. In this state some of the magnetic field is allowed to penetrate into the material and influence the internal magnetic structure causing parts of it to become antiferromagnetic. This state ends at a second critical field H_{c2} and leads into the third state which is the same as the second state for Type I superconductors. Figure 3 shows the general relationship between temperature and magentic field for a Type II superconductor.

2.2 The Superconductor YBCO

The Type II superconducting material YBCO is one of the most studied high T_c materials currently known. Having a critical temperature of 92 K before entering a non-superconductive state, about an order of magnitude higher than most Type I Superconductors, makes experimentation much easier to accomplish than most other

Type II materials. The unit cell crystal lattice is shown in Figure 1. In the unit cell crystal, the $Cu - O - Cu$ chains that line the b axis of the cell correspond to the B direction in the material and the CuO_2 planes that lie between the two Barium and one Yttrium atoms are thought to be the source of the superconductivity of the material. The superconducting currents tend to favor flowing in a direction parallel to these planes and have a much harder time flowing in directions perpendicular to them due to the much larger effective charge carrier mass required in this orientation. The charge carrier masses within the planes parallel to the a and b axes are both represented by the single mass M_1 because of the lack of anisotropy between these two directions. The charge carrier mass perpendicular to the planes corresponds to the c axis and is represented by the mass M_3. The anisotropy parameter Γ for YBCO is found by calculating the ratio between masses m_3 and m_1

$$\Gamma = \frac{m_3}{m_1} \tag{1}$$

where $m_3 = \frac{M_3}{M_{av}}, m_1 = \frac{M_1}{M_{av}}$, and $M_{av} = (M_1^2 M_3)^{\frac{1}{3}}$. For simplicity's sake the anisotropy factor for YBCO has been calculated to be 25. This factor is useful when the anisotropic fitting function is used. This fitting function is discussed in further detail in section 3.

3 Experimental Setup and Analysis

3.1 The OMNI Setup

A typical setup for a μSR experiment area with anisotropic superconductors is shown in Figure 4 below.

As the muons travel individually down the beam line to the target area they pass through the muon signal screen which prevents all other beam contents from entering the sample. They then proceed to the target sample and, if succesful, enter it. Upon

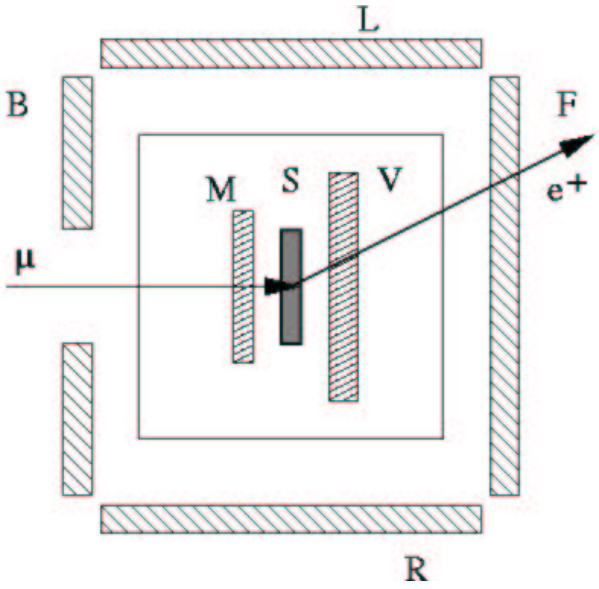

Figure 4: A typical setup for a μSR experiment. S represents the target sample; M is the muon signal screen; V is the veto filter; L, B, R, and F are the left, back, right, and front detectors; and μ is the muon beam line.

entering the sample the muons then precess in the internal magnetic fields and begins to lose energy by ionizing atoms and scattering electrons. When the muon reaches a critical energy of 15 eV it undergoes the decay reaction

$$\mu^+ \rightarrow e^+ + \nu_e + \overline{\nu}_\mu \tag{2}$$

where ν_e is the neutrino associated with electrons and $\overline{\nu}_\mu$ is the anti-neutrino associated with the muon. The resulting positrons exit the decay in the same direction as the muon's spin at the time of decay and are recorded by several detectors placed around the sample. From the data recorded by the detectors assymetry plots are made that reveal the influence of the internal magnetic fields on the muon's orientation at the time of decay.

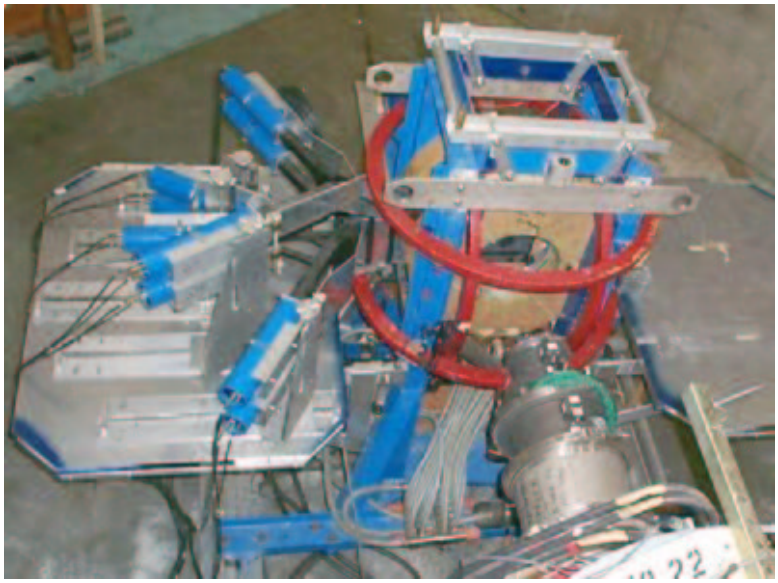

Figure 5: The OMNI apparatus at TRIUMF

3.2 Analysis of the Data

To handle the arduous task of analyzing the data recorded by the detector pairs Dr. Kossler designed a Fortran program that utilizes several different fitting functions ranging from simple Gaussians to complex anisotropic equations stemming from the London Approximation. Some of the functions used are useful only for certain scenarios such as the London Theory isotropic fitting function which is used only when the external magnetic field is parallel to the c axis of the material. To begin, the internal magnetic field components of the Flux Line Lattice unit cell, abbreviated FLL, are written in real space as [1]:

$$b_x - \lambda^2(m_{zz} \bigtriangledown^2_{xy} b_x - m_{xz}\frac{\delta^2 b_z}{\delta y^2}) = 0 \tag{3}$$

$$b_y - \lambda^2(m_{zz} \bigtriangledown^2_{xy} b_y - m_{xz}\frac{\delta^2 b_z}{\delta z \delta y}) = 0 \tag{4}$$

$$b_z - \lambda^2(m_1\frac{\delta^2 b_z}{\delta x^2} + m_{xx}\frac{\delta^2 b_z}{\delta y^2} - m_{xz} \bigtriangledown^2_{xy} b_x) = \Phi_0 \sum_{\nu} \delta(\mathbf{r} - \mathbf{r}_\nu) \tag{5}$$

where $\bigtriangledown^2_{xy} = \frac{\delta^2}{\delta x^2} + \frac{\delta^2}{\delta y^2}$ is the two dimensional Laplacian in the xy plane, $\mathbf{r}$ is a vector in the FLL, and $\mathbf{r}_\nu$ are the vectors of the vortices.

Assuming that the vortices in the material are well spaced and do not overlap these equations can then be put through a Fourier transform and summed in Fourier space. The Fourier relationship for this procedure is

$$b(r) = \sum_{\mathbf{G}} b(\mathbf{G}) e^{i\mathbf{G}\cdot r} \tag{6}$$

$$b(\mathbf{G}) = \frac{B}{\Phi_0} \int b(r) e^{-i\mathbf{G}\cdot r} dr \tag{7}$$

where $\mathbf{G}$ are the reciprocal lattice vectors and B is the magnitude of the average field over the real space FLL unit cell. The integral is taken over the unit cell in real space.

Inserting $b(r)$ into the component equations gives the field components in terms of the reciprocal lattice vectors

$$b_x(\mathbf{G}) = B\lambda^2 m_{xz} G_y^2 / d \tag{8}$$

$$b_y(\mathbf{G}) = -B\lambda^2 m_{xz} G_x G_y / d \tag{9}$$

$$b_z(\mathbf{G}) = B(1 + \lambda^2 m_{zz} G^2) / d \tag{10}$$

with the denominator d equal to:

$$d = (1 + \lambda^2 m_1 G_x^2 + \lambda^2 m_{xx} G_y^2)(1 + \lambda^2 m_{zz} G^2) - \lambda^4 m_{xz}^2 G^2 G_y^2 \tag{11}$$

Transforming these equations back into real space gives the real space magnetic field components of a general point in the FLL. Summing these points in the FLL gives a general structure to the fields in the unit cell. Summing the unit cells then gives a general structure of the fields in the sample. For this summation a subroutine in the fitting program named *hsumag*37 is used.

```
      subroutine hsumag37(B,b1,b2,dx,dy, xlab,xi,hsum,
     $ INDEX,theta,Gamma,psi)
      implicit none
      integer IG,INDEX
      real pi,phi0,Gamma,theta
      parameter (pi=3.141592654,phi0=2.07e3,IG=50)
      real B,xlab,xi,hsum(1:3,0:INDEX,0:INDEX)
      real gx(-IG:IG,-IG:IG),gy(-IG:IG,-IG:IG)
      real hg(1:3,-IG:IG,-IG:IG)
      real m1,m3,mxx,myy,mxz,mzz,psi
      integer i,j,k,l,m
      real b1,b2,dx,dy,xls,gs,d,rx,ry,xl
      xl=xlab*Gamma**(1./6.);xls=xl*xl
      call setstuff37(B,b1,b2,gx,gy,m1,m3,mxx,myy,mxz,mzz,theta,
     $Gamma,psi)
c Fields in Rec. Lattice
      do i=-IG,IG
         do j=-IG,IG
            gs=gx(i,j)**2+gy(i,j)**2
            d=(1+xls**m1*gx(i,j)**2+xls*mxx*gy(i,j)**2)*(1+xls*mzz*gs)-
     $           xls*mxz*gs*gy(i,j)**2
            hg(1,i,j)=B*xls*mxz*gy(i,j)**2/d
            hg(2,i,j)=-B*xls*mxz*gx(i,j)*gy(i,j)/d
            hg(3,i,j)=B*(1+xls*mzz*gs)/d
         enddo
      enddo
c Fields in Dir. Lattice
```

```
 do i=0,INDEX
    do j=0,INDEX
       hsum(3,i,j)=B;hsum(1,i,j)=0.;hsum(2,i,j)=0.
       rx=dx*i
       ry=dy*j
       do k=1,3
          do l=1,IG
 hsum(k,i,j)=hsum(k,i,j)+2.*hg(k,l,0)*cos(rx*gx(l,0)+ry*gy(l,0))+
$                    2.*hg(k,0,l)*cos(rx*gx(0,l)+ry*gy(0,l))
             do m=1,IG
 hsum(k,i,j)=hsum(k,i,j)+2.*hg(k,l,m)*cos(rx*gx(l,m)+ry*gy(l,m))+
$                   2.*hg(k,l,-m)*cos(rx*gx(l,-m)+ry*gy(l,-m))
             enddo
           enddo
       enddo
    enddo
 enddo
 return
 end
```

4 Experimentation with the Superconductor YBCO

4.1 Background

Initial work on the structure of the current vortices handled the sceanrio of "Pancake" vortices, individual vortices stacked one on top of the other like a stack of pancakes. [2] This method served as a foundation for further work with current vortices in superconductors but this does not apply to the Type II superconductor this experiment

works with. For YBCO, three regimes of flux density are identified. These regimes are defined by the magnitude of the applied external field relative the to critical field values of the sample. The first regime encompasses all values of B near H_{c1} when the vortices are spaced well apart. The second regime encompasses moderate values of B between H_{c1} and H_{c2} when the spacing between the vortices decreases. The third regime encompasses values of B near H_{c2} when the vortices are overlapping. For this experiment the value of B lies within the second regime. To get a better understanding of the field structure around these vortices the local flux density in a plane perpendicular to the field is put through a Fourier series. Michael Tinkham presents in his book $Introductionto Superconductivity$ that the series for this procedure is [3]

$$h_z(\mathbf{r}) = \sum_{\mathbf{Q}} h_{\mathbf{Q}} e^{i\mathbf{Q}\cdot\mathbf{r}} \tag{12}$$

where Q represents the reciprocal lattice vectors and H_Q the reciprocal field. You may notice a distinct similarity between this Fourier series and the Fourier series discussed in the previous section. Assuming that the translation coordinates for a triangular array of vortices are not orthogonal the relationship between h_Q and the reciprocal lattice vectors becomes

$$\sum_{\mathbf{Q}} (h_{\mathbf{Q}} + \lambda^2 Q^2 h_{\mathbf{Q}}) e^{i\mathbf{Q}\cdot\mathbf{r}} = B \sum_{\mathbf{Q}} e^{i\mathbf{Q}\cdot\mathbf{r}} \tag{13}$$

Solving for h_Q and plugging that back into the Fourier series gives the general field distribution

$$h_z(\mathbf{r}) = B \sum_{\mathbf{Q}} \frac{e^{i\mathbf{Q}\cdot\mathbf{r}}}{1 + \lambda^2 Q^2} \tag{14}$$

for the longitudenal component plane perpendicular to the field B and the vortex axes.

Further investigation performed by S. Thiemann, Z. Radovic, and V. Kogan shows that this is the case for the longitudinal components of the field for large fields. However, the transverse field components do not lie within a plane perpendicular to the vortex axes.[4] Rather, they lie within a plane skewed by a rotation α about the y axis in the xy plane.

For low field values a different approach was taken by L. Daemen, L. Campbell, and V. Kogan. This approach uses the London Approximation to determine the geometry of the FLL for low fields and theorizes that the lattice parameters a and b, equivalent to $b1$ and $b2$ in other sources, depend greatly on the orientation of the external field relative to the c axis of the sample. Daemen, Campbell, and Kogan show that the lattice parameters and the angle between them, ψ, have the following relationships with the ratio of the flux lattice parameter ρ [5]:

$$a = (\frac{\Phi_0}{B}\frac{\rho}{[1-(\rho/2)^2]^{\frac{1}{2}}})^{\frac{1}{2}}, \tag{15}$$

$$b = (\frac{\Phi_0}{B}\frac{1}{\rho[1-(\rho/2)^2]^{\frac{1}{2}}})^{\frac{1}{2}}, \tag{16}$$

$$cos\psi = \frac{\rho}{2}. \tag{17}$$

From these relationships, they further theorize that when the angle between the field and the c axis, θ, approaches $\pi/2$ that ψ also approaches $\pi/2$ and the lattice paramter a becomes much smaller than b creating what has been termed "Flux Line Pairs" or rows of vortices parallel to one another.

4.2 Low External Field Parallel to the c Axis

For the first set of data, a small external magnetic field of 0.5 G was introduced to the superconductor. This magnetic field was oriented parallel to the polarization axis of the superconducting layers and the temperature was varied from 10K to 91K. However, due to anti-ferromagnetic interference around 85K, further analysis past this

temperature was rendered extremely difficult. The positron detector pair left/right was used for the construction of the asymmetry plots. A simple four parameter Guassian function, $e^{\frac{-\sigma^2 t^2}{2}}$, was used to get a feel for some starting values to the amplitude and frequency. Then an isotropic fitting function such as:

$$a[f_s a_s(t) + (1 - f_s)e^{-\sigma^2 t^2/2}] + a_{dc}e^{-t/t_{dc}} \tag{18}$$

where $a_s(t) = \int cos(\omega t + \phi)d\omega$ was used to map the changes to certain parameters in better detail.

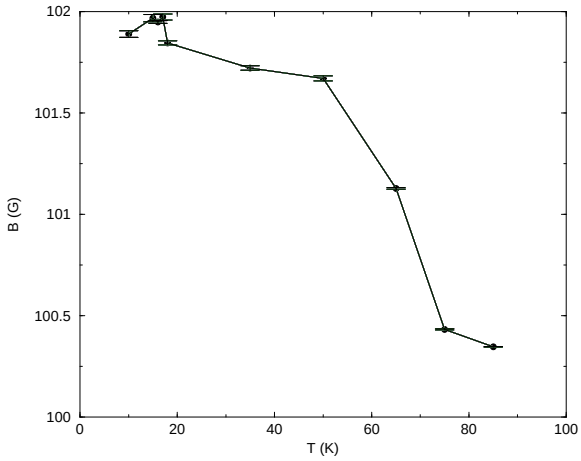

Figure 6: Internal Field, B, as a function of Temperature, T.

In Figure 6 we see the behavior of the magnetic field inside the conductor versus the temperature, T. As the temperature steadily increases the field decreases dramatically as more and more of the current vortices in the layers of the superconductor decouple and the material turns antiferromagnetic. Also, around the temperature of 17K there is a marked jump in magnitude of the internal field. After this point the field begins to decline as stated earlier. This marks the threshhold of superconductivity for the material at low temperatures.

In Figure 7 we see how the background field drops off as the material becomes increasingly antiferromagnetic around the temperatures of 15K and 86K. Also worth

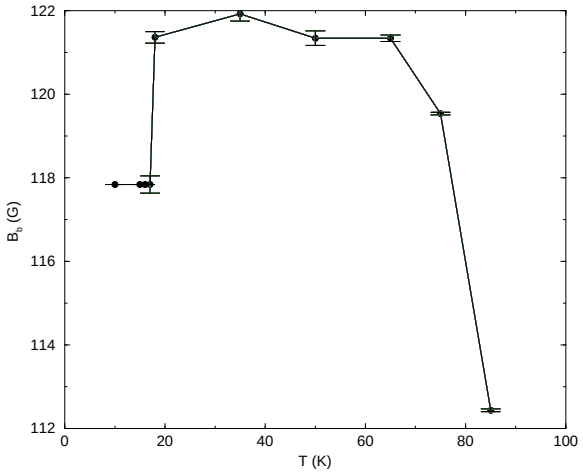

Figure 7: Background field, Bb, as a function of T.

noting is how the field remains relatively constant while in this range of temperatures. This is due to the admittance of the external field into the material and the subsequent creation of the current vortices in the superconducting layers..

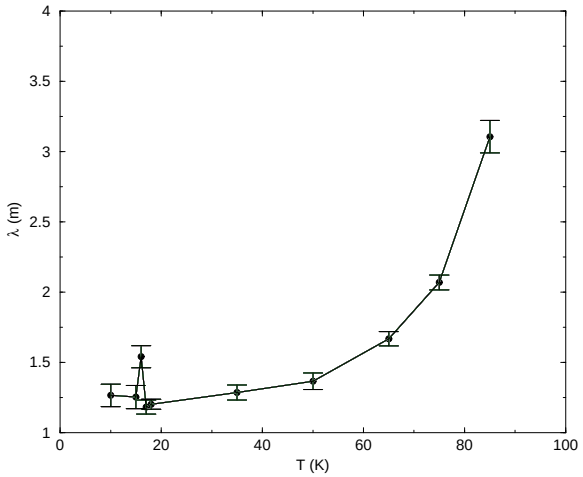

Figure 8: Penetration depth as a function of Temperature.

For the penetration depth of the sample we see almost an exponential increase with higher temperatures. Starting at 15K we have a depth of 1.3-1.4 nanometers. As the temperature increases past the superconducting threshhold, the penetration depth increases above 2 nm and even up to 3 nm. As the temperature increases, so does the penetration depth of the material until it goes to, theoretically, infinity at

the non-superconducting threshold of the material. The increase in penetration depth spurs the spacing between the vortices to shrink to the point where the vortex cores overlap and they decouple. In Figure 8 the penetration depth versus the temperature is shown.

The isotropic fitting function gave us a starting point when interpretting the behaviors of the parameters of the material, but to finish the job a more complex anisotropic fitting function that incorporated the angle geomtery of the scenraio, the anisotropy parameter, and the factor ψ based off of Daemen, Campbell, and Kogan's work was implemented. After all, YBCO is an anisotropic Type II superconductor and such a function would generate, in theory, better results. The variable ψ is calculated by finding the value for the parameter ρ which is discussed in their work. For this specific scenario, ρ is 1. Using this as well as θ, the angle between the external field and the c axis, and α, the angle between the polarization of the vortices and the y axis, along with Γ the set of data was mapped again and plots of the same parameters generated.

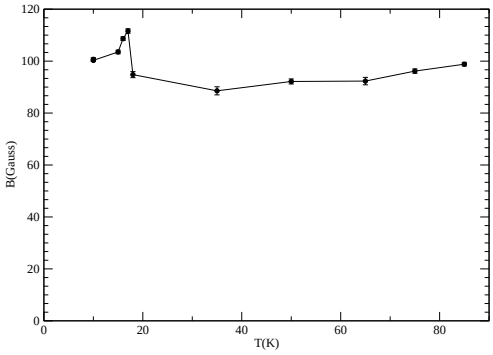

Figure 9: Internal Field as a function of Temperature after having used the anisoptropic fitting functon.

For the internal field we see a relatively constant value across the range of temperatures which varies from the plot generated by the isotropic function. This is due

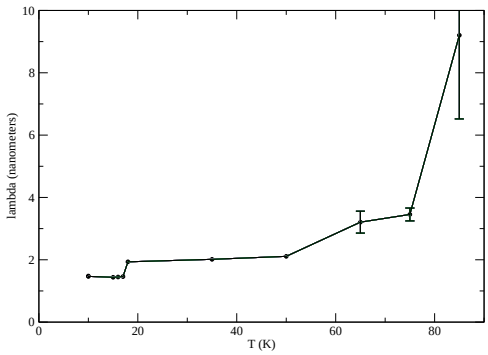

Figure 10: The penetration depth λ as a function of T after having used the anisotropic fitting function

to the field being considered entirely longitudinal relative to the c axis.

For the penetration depth we see a bahavior similar to the one mapped by the isotropic function. As the temperature steadily rises, the penetration depth also rises and eventually increases to infinity when the material becomes non-superconducting.

4.3 Low External Field Perpendicular to the c Axis

The next set of data covers the scenario of an external field perpendicular to the c axis of the crystal. For this set, the isotropic fitting function used in the previous section is not appropriate due to its lack of angle dependency and inability to fit for the transverse components of the field relative to the c axis. Simply put, the function always considers θ to be zero. The second fitting function, the anisotropic function with angle dependency, is still useable and provides interesting results. The variable ρ in this case is considered to be .23. The external field is still .5 G and the sample is put through the same range of temperatures used in the previous case.

The behavior of B in this scenario mimics that of B in the previous case and reflects that now the entire field is transverse to the c axis. The function adjusts for this fact. For the penetration depth one would expect to see an agreement between this case and

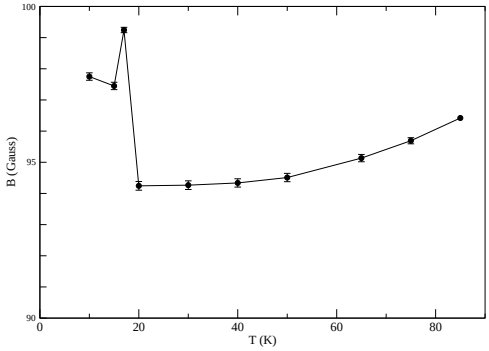

Figure 11: The internal field as a function of T for the case of B⊥c.

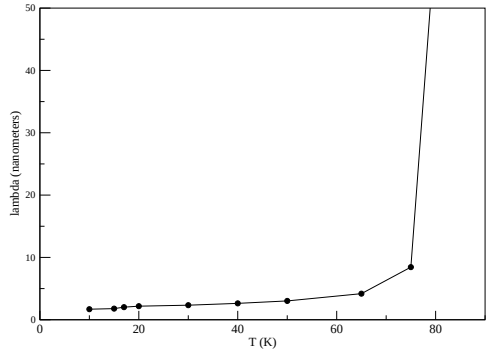

Figure 12: The penetration depth as a function of T for the same case.

the longitudinal case. From the plot of the penetration depth we see that this is the case. This agreement between the two scenarios points to the possible formation of "Flux Line Pairs" as theorized by Daemen, Campbell, and Kogan. As the transverse components of the field increase relative to the c axis, the two FLL parameters a and b become exceedingly anisotropic relative to one another. The parameter b becomes much larger than a and the triangular lattice pattern takes on the appearence of two parallel lines of vortices.

4.4 Low External Field at a 45° angle to the c Axis

For the final set of data, the sample is kept at a constant 110 K but minor variations to the orientation in the magnetic field are implemented. Starting from a 45° angle to the c axis, the external field's y component is increased in small increments. The external field's overall magnitude is 100 G, relatively large compared to the other two sets. For YBCO this temperature reaches far into the non-superconducting state and the external magnetic field is able to penetrate through the sample giving a great degree of feedom in manipulating the field structure internal to the material. However, due to time constraints this set is not fully analyzed and requires further investigation.

5 Conclusions

While the initial investigation using the London Theory isotropic fitting function revealed disparities between the cases of a field parallel to the c axis and a field perpendicular to the c axis, the subsequent use of the angle-dependent anisotropic fitting function showed a great deal of agreement between their penetrations depths. The implementation of the variable ρ that Daemen, Campbell, and Kogan used to explain the interdependence of the FLL componenets a and b and the angle θ fixed any irregularities in the mapping of the two cases. This could indeed be the first physical evidence of the formation of "Flux Line Pairs" in the B$\perp$c scenario. Further experimentation and analysis of these cases as well as the the case of B at a 45° angle to the c axis is needed to strengthen this claim.

References

[1] A. J. Greer and W. J. Kossler, *Low Magnetic Fields in Anisotropic Superconductors* (Springer, Berlin, 1995).

[2] J. R. Clem, Phys. Rev. B **43**, 7837 (1991).

[3] M. Tinkham, *Introduction to Superconductivity* (McGraw-Hill, Inc., New York, 1996).

[4] S. L. Thiemann, Z. Radovic, and V. G. Kogan, Phys. Rev. B **39**, 406 (1989).

[5] L. L. Daemen, L. J. Campbell, and V. G. Kogan, Phys. Rev. B **46**, 3631 (1992).